DINAME 2023 - Proceedings of the XIX International Symposium on Dynamic Problems of Mechanics,
A.S. De Paula, A.T. Fabro and M.R. Machado (Editors), ABCM.
Pirenópolis, Go, Brazil, February 26th to March 3rd, 2023

Low-cost inertial sensor fusion with the Ensemble Kalman filter for ground vehicle position estimation

Enrico Bertolini Carlini[1], **Agenor de Toledo Fleury**[1], **and Flavio Celso Trigo**[1]

[1] Escola Politecnica da USP

Av. Prof. Mello Moraes – 2231 – 05508-970 – São Paulo – SP – BRASIL

Abstract: Usually, the position of ground vehicles is obtained from the Global Navigation Satellite System (GNSS), which is a source of reliable estimates; however it is prone to signal loss specially in dense urban areas, where buildings shadow the direct reception of satellite signals. An alternative to overcome this drawback is dead reckoning: Integration of low-cost encapsulated inertial measurement units' (IMUs) signals (angular velocity, from gyro, and acceleration, from accelerometer) in order to estimate the target position. This method, however, results in error build-up due to model uncertainties and measurement noise. Therefore, the research on an uninterrupted and trustworthy estimation method is relevant to the navigation field. In this work, we implement a non-linear discrete quaternion-based model to describe the kinematics of a rigid body with six degrees of freedom and apply the Ensemble Kalman filter (EnKF) to fuse IMU sensors' signals and perform dead-reckoning. The estimation method is evaluated in a field test with a passenger car travelling on a 370*-meter long closed trajectory. Measurements of linear and angular velocities, and barometric pressure, are the observations processed by the EnKF, whose estimates are compared with ones from the Unscented Kalman filter (UKF). The EnKF position estimation discrepancy on the departure/arrival locus was* 2 *m, whereas the maximum error along the track was* 8 *m. Those preliminary results suggest that the EnKF might be a viable option to perform dead-reckoning. We currently seek to optimise the EnKF estimates by fusing data from several IMUs.*

Keywords: data fusion, dead reckoning, Ensemble Kalman filter, stochastic parameter estimation, inertial sensors

INTRODUCTION

The position of a ground vehicle can be tracked externally, with the Global Navigation Satellite System (GNSS), or internally, performing dead reckoning with data from inertial sensors (Kochem *et al.*, 2002). The GNSS is comprised by an array of satellites whose signals are received by the vehicle and used to estimate its position on the globe. This method's accuracy is smaller than 3.5 meters, but only if there are at least four satellites in the field of view of the vehicle, which is not always the case (Oxley, 2017).

On the other hand, dead reckoning is based on a mathematical model to propagate data from inertial sensors in the vehicle (such as rate-gyros and accelerometers) and estimate their displacement and heading, thus determining a new position in relation to a previous one. There are two main kinds of such sensors: gymbal-based and strap-down based. The former are very accurate and expensive, whereas the latter, produced in large scale as microelectromechanical systems (MEMS) named Inertial Measurement Units (IMUs) are cheap, though far less accurate.

The propagation of vehicle kinematics deterministic model without taking into consideration the intrinsic noisy nature of measurement sensors, and of the uncertainties on the assumed vehicle model itself, leads to cumulative non-acceptable errors for practical purposes (Shit, 2020). Among the sources of sensor's errors, it is worth citing *bias* (a quasi-constant output component that is independent of the input), *drift* (caused by sensor temperature variation), *quantization* (effect related to the discretization of continuous signals), and *misalignment* (in case sensor triad is not orthogonal within admissible limits). This drawback can be properly overcome by addressing measurement and system (the vehicle) model uncertainties within a stochastic estimation framework as additive random noise. One of the tools available to perform this task and improve estimate's accuracy is through Kalman filters (Sabattini, 2009).

Accurate tracking moving targets is a major challenge in dead reckoning, specially when only low-cost strap-down sensors are available; particularly in vehicle tracking, the extended Kalman filter has been employed for sensor fusion of signals from several sources in order to improve the overall measurement accuracy. For instance, Park & Hong (2011), state that, with a minimum of 12 accelerometers in IMU's, it is possible estimate attitude without performing numerical integration, although the authors do not present results validation. Other recent works that employ Kalman filters to combine information from low-cost IMUs (Vargas-Melendez et al., 2017, Al-Shabi & Bonny, 2022) report estimates convergence difficulty when non-linear models are used to describe system dynamics. In order to deal with issues related to non-linearity of the model, Scholte et al. (2019), and Marco et al. (2020), include an assumed dynamic for additive sensor noise; according to the authors, this approach allows the estimation of 6 degree-of-freedom IMUs drift when combined with information from other sensors such as vehicle height, steer angle and, wheel rotation; for supervision and correction, GPS signals are still necessary. Thus, despite those efforts, adequate position estimation in real time with low-cost strap-down sensors is an up-to-date research topic.

Considering the above scenario, in this work our aim is to fuse data from low-cost strap-down IMU sensors commonly available in passenger cars to obtain accurate estimates of vehicle position. Fusion of acceleration, magnetic Earth field, yaw-rate and velocity measurements obtained in an experiment with a passenger car is made through the Ensemble Kalman filter (EnKF) and the Unscented Kalman filter (UKF), whose results are presented and compared. To our best knowledge, the EnKF in this application with real data poses a contribution.

THEORETICAL BACKGROUND

Mathematical model

In order to helping the development of vehicle kinematic model, two frames of reference are adopted: one rigidly linked to the vehicle (X,Y,Z) , called the moving non-inertial reference frame ($\mathscr{B}$-frame), and another (X^e,Y^e,Z^e), fixed to the surface of Earth, called the fixed inertial reference frame ($\mathscr{E}$-frame), as depicted in Fig. 1. The displacements and velocities of the car are represented in vector form as

$$\mathbb{x} = [x\ y\ z]^t; \quad \boldsymbol{u} = [u\ v\ w]^t; \quad \boldsymbol{\phi} = [\phi\ \theta\ \psi]^T; \quad \boldsymbol{p} = [p\ q\ r]^t, \quad t \equiv \text{matrix transpose}, \tag{1}$$

whose meaning are defined in Tab. 1.

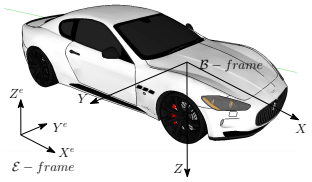

Figure 1: Earth and body reference frames.

Table 1: Displacements and velocities with respect to adopted reference frames.

Ref. frame: $\mathscr{B}$ / $\mathscr{E}$	Unit vector	Displacement (m) or (rad)	velocity (m/s) or (rad/s)	Orientation
X/X^e	$\boldsymbol{i}/\boldsymbol{i}^e$	x/x^e	u/u^e	$(+)$ front
Y/Y^e	$\boldsymbol{j}/\boldsymbol{j}^e$	y/y^e	v/v^e	$(+)$ right
Z/Z^e	$\boldsymbol{k}/\boldsymbol{k}^e$	z/z^e	w/w^e	$(+)$ down
around X	$\boldsymbol{i}$	ϕ	p	
around Y	$\boldsymbol{j}$	θ	q	right-hand rule
around Z	$\boldsymbol{k}$	ψ	r	

Reference frames alignment for determination of the direction cosine matrix between $\mathscr{B}$ and $\mathscr{E}$ frames is obtained through the TRIAD algorithm (Sabattini, 2009), as briefly described next. First of all, one takes two linearly independent vectors that are known in $\mathscr{E}$-frame but represented in $\mathscr{B}$-frame coordinates, for instance $\mathbf{v}_1$, $\mathbf{v}_2$, which are named *reference* vectors. Next, the same vector quantities are measured by the sensor strapped to the vehicle and represented in the same $\mathscr{B}$-frame coordinates, for instance, $\mathbf{w}_1$ and $\mathbf{w}_2$, which are called *observation* vectors. Then, unit vectors are calculated as

$$\mathbf{m}_1 = \frac{\mathbf{v}_1}{||\mathbf{v}_1||}; \quad \mathbf{m}_2 = \mathbf{m}_1 \wedge \frac{\mathbf{v}_2}{||\mathbf{v}_2||}; \quad \mathbf{m}_3 = \mathbf{m}_1 \wedge \mathbf{m}_2 \quad \mathbf{n}_1 = \frac{\mathbf{w}_1}{||\mathbf{w}_1||}; \quad \mathbf{n}_2 = \mathbf{n}_1 \wedge \frac{\mathbf{w}_2}{||\mathbf{w}_2||}; \quad \mathbf{n}_3 = \mathbf{n}_1 \wedge \mathbf{n}_2 \tag{2}$$

in which "$\wedge$" denotes the cross vector product. Finally, the direction cosine matrix $C^{E\to B}$ from $\mathscr{E}$ to $\mathscr{B}$ is calculated according to

$$C^{E\to B} = [\mathbf{m}_1 \quad \mathbf{m}_2 \quad \mathbf{m}_3] \cdot [\mathbf{n}_1 \quad \mathbf{n}_2 \quad \mathbf{n}_3]^t, \tag{3}$$

with "$\cdot$" standing for matrix product. In this work, quaternions, given by

$$\mathbf{q} = [q_0 \quad q_1 \quad q_2 \quad q_3]^t \ \Big|\ \|\mathbf{q}\| = \sqrt{q_0^2+q_1^2+q_2^2+q_3^2} = 1, \tag{4}$$

are used to describe the direction cosine matrix, $C(\mathbf{q})$, as

$$C(\mathbf{q}) = \begin{bmatrix} q_0^2+q_1^2-q_2^2-q_3^2 & 2q_1q_2-2q_0q_3 & 2q_1q_3+2q_0q_2 \\ 2q_1q_2+2q_0q_3 & q_0^2-q_1^2+q_2^2-q_3^2 & 2q_2q_3-2q_0q_1 \\ 2q_1q_3-2q_0q_2 & 2q_2q_3+2q_0q_1 & q_0^2-q_1^2-q_2^2+q_3^2 \end{bmatrix}. \tag{5}$$

The differential equation to be solved for the time evolution of the quaternion $\mathbf{q}$ as function of the angular velocity (gyro measurement) vector $\mathbf{p}$ is

$$\dot{\mathbf{q}} = \frac{1}{2}\begin{bmatrix} 0 \\ \mathbf{p} \end{bmatrix} \otimes \mathbf{q} = \frac{1}{2}\begin{bmatrix} 0 & -p & -q & -r \\ p & 0 & r & q \\ q & -r & 0 & p \\ r & q & -p & 0 \end{bmatrix} \cdot \mathbf{q} = \frac{1}{2}\mathbf{W}(\mathbf{p}) \cdot \mathbf{q}, \quad \text{with } \otimes \equiv \text{ quaternion product.} \tag{6}$$

The differential equation for the acceleration of the vehicle is obtained by the time derivative of the velocity $\mathbf{u}^e$ described in coordinates of the $\mathscr{B}$-frame with respect to the $\mathscr{E}$-frame, which is also a function of the $\mathbf{p}$ vector. The acceleration of gravity is subtracted from the IMU acceleration vector measurement, $\mathbf{a} = [a_x \quad a_y \quad a_z]^t$, and results in

$$\dot{\mathbf{u}} = \mathbf{a} - C^t(\mathbf{q}) \cdot \mathbf{g} - \mathbf{J}(\mathbf{p}) \cdot \mathbf{u}, \quad \text{in which} \quad \mathbf{J}(\mathbf{p}) = \begin{bmatrix} 0 & -r & q \\ r & 0 & -p \\ -q & p & 0 \end{bmatrix}. \tag{7}$$

With Eqs. (6) and (7), and the discretization interval T, the discrete-time state-space non-linear kinematic model of the vehicle is given by

$$\begin{gathered} \mathbb{x}_k = \boldsymbol{f}_k(\mathbb{x}_{k-1}, T) \\ \begin{bmatrix} \mathbf{q} \\ \mathbf{u} \\ \mathbf{x}^e \\ \boldsymbol{\phi} \end{bmatrix}_k = \begin{bmatrix} \mathbf{q} \\ \mathbf{u} \\ \mathbf{x}^e \\ \boldsymbol{\phi} \end{bmatrix}_{k-1} + \begin{bmatrix} \frac{1}{2}\mathbf{W}(\mathbf{p}_{k-1}) \cdot \mathbf{q}_{k-1} \\ \mathbf{a}_k - C^t(\mathbf{q}_{k-1}) \cdot \mathbf{g} - J(\mathbf{p}_{k-1}) \cdot \mathbf{u}_{k-1} \\ C(\mathbf{q}_{k-1}) \cdot \mathbf{u}_{k-1} \\ \mathbf{p}_{k-1} \end{bmatrix} T \end{gathered} \tag{8}$$

Kalman filters

The state of a system is theoretically obtained by propagating an analytic model, such as Eq. (8), from a supposedly known initial state and possibly taking measurements related to the state as inputs. In real life applications, this approach is prone to unaccounted errors either from inherent measurement noise or from assuming that the analytic model accurately mimics the actual system. One of the possibilities to dealing with the aforementioned issues is through Kalman filters, since their stochastic nature can accommodate uncertainties from both system and measurement models. An extensive discussion on Kalman filters is available in the literature as, for instance, (Maybeck, 1979), and several others; for the moment, it suffices to mention that the basic structure of Kalman filtering involves two successive iterative steps: first, in the absence of new information from sensors, the current state is propagated with the analytic model in order to obtain an *a priori* estimate of the state-vector; then, when new information (*i.e.*, measurement data) is available, the state is updated taking into account system model and measurement errors to provide an optimal (linear model) or sub-optimal (non-linear model) *a posteriori* estimate of the state.

In this work we adopt the non-linear discrete function $\boldsymbol{f}_k$ of the state $\mathbb{x}_k \in \mathscr{R}^{13}$ of Eq. 8 as the vehicle (plant) kinematic model and a linear discrete function $\mathbb{y}_k \in \mathscr{R}^4$ of the state as the observation model. Both of them are affected by additive independent white noise sequences $\boldsymbol{\omega}_k \in \mathscr{R}^{13}$ and $\boldsymbol{\nu}_k \in \mathscr{R}^4$ with known probability density functions and covariance matrices Q and R that represent the uncertainties in plant and observation models. Thus, the complete system in proper framework for Kalman filter implementation is given by the following equations:

$$\mathbb{x}_k = \boldsymbol{f}_k(\mathbb{x}_{k-1}, T) + \boldsymbol{\omega}_{k-1} \tag{9}$$

$$\mathbb{y}_k = H\mathbb{x}_k + \boldsymbol{\nu}_k, \text{ with } \mathbb{y}_k = [u\ v\ w\ z^e]^t, \tag{10}$$

and $H \in \mathscr{R}^{13x4}$ with ones at the proper spots and zeros elsewhere. It is noteworthy to mention that velocities v and w are not effectively measured by the Hall sensor. Certainly, some side and vertical motion, although small, exist; however, it is a fair hypothesis to consider their effect as *perturbations*, and include them in Kalman filter framework as zero-mean Gaussian noise with $0.1\ m/s$ standard deviation. The EnKF and the UKF, which will fuse Hall, barometer and UMI sensors to estimate the state, are briefly presented next.

Ensemble Kalman filter – EnKF

Since the actual statistics of the state is unknown, the EnKF, as proposed by Evensen (2003), takes a random *ensemble* of N "points" (state-vectors, called "particles") of the n-dimensional space and propagate them through the non-linear model (as opposed to the linearized versions of the KF). The error of evaluating a sample of N instead of the whole population decreases at a $1/\sqrt{N}$ rate; thus, as $N \to \infty$, the probability density function (*pdf*) of the realisations tends to the actual one. Once this *pdf* is available, all moments of the distribution can be computed. This is the essence of the EnKF.

Computational implementation starts with a matrix of estimates (denoted by the "$\hat{}$" sign) $\hat{\mathbb{X}}_{k-1}^{+} = \{\hat{\mathbf{x}}_1 \ \hat{\mathbf{x}}_2 \ \ldots \hat{\mathbf{x}}_N\} \in \mathscr{R}^{n\times N}$ whose columns contain the $\hat{\mathbf{x}}_j,\ j = 1,\ldots,N$ *ensemble* vectors updated at the $k-1$-*th* iteration. The uncertainties of the model are included in each vector of the *ensemble* as additive Gaussian white noise with covariance matrix Q. Until the arrival of the next observation data, this *ensemble* is propagated through the non-linear plant model, resulting in the *a priori* estimated state, $\hat{\mathbb{X}}_k^-$. Then, the mean state *ensemble* matrix $\hat{\bar{\mathbb{X}}}_k^-$, the perturbation matrix $\boldsymbol{\delta}\hat{\mathbb{X}}_k^-$ and the *ensemble* state-error covariance matrix $\mathbb{P}_k^-$ are calculated by

$$\hat{\bar{\mathbb{X}}}_k^- = \hat{\mathbb{X}}_k^- \cdot I_N; \qquad \boldsymbol{\delta}\hat{\mathbb{X}}_k^- = \hat{\mathbb{X}}_k^- - \hat{\bar{\mathbb{X}}}_k^- \qquad \mathbb{P}_k^- = \frac{1}{N-1}\boldsymbol{\delta}\hat{\mathbb{X}}_k^- \left(\boldsymbol{\delta}\hat{\mathbb{X}}_k^-\right)^t \tag{11}$$

When the next measurement vector $\mathbf{y}_k$ is received, the observation *ensemble* $\mathbb{Y}_k \in \mathscr{R}^{p\times N}$ is built, in a similar manner as the *ensemble* state vector, with the inclusion of additive Gaussian white noise with covariance matrix R. Then, the updated *ensemble* state matrix $\hat{\mathbb{X}}_k^+$ is computed according to

$$\hat{\mathbb{X}}^+ = \hat{\mathbb{X}}^- + \delta\hat{\mathbb{X}}\delta\hat{\mathbb{X}}^t H^t \left(H\delta\hat{\mathbb{X}}\delta\hat{\mathbb{X}}^t H^t + EE^t\right)^{-1}\left(\mathbb{Y}_k - H\hat{\mathbb{X}}_k\right), \tag{12}$$

with $E = \{\boldsymbol{\nu}_1 \ \boldsymbol{\nu}_2 \ \ldots \boldsymbol{\nu}_N\} \ \in \mathscr{R}^{p\times N}$. Finally, the updated state $\hat{\mathbf{x}}_k^+$ is the mean of the *ensemble* vectors in matrix $\hat{\mathbb{X}}^+$ from Eq. (12).

Unscented Kalman filter – UKF

The UKF, introduced by Julier and Uhlmann (1997), is also aimed at reducing the linearization errors of the classical KF versions. For a state with dimension n, a collection of $2n$ state samples known as *sigma points* are obtained by

$$\hat{\mathbb{X}}_{k-1}^{(i)} = \Delta\mathbb{X}^{(i)} + \hat{\mathbb{X}}_{k-1}^{+},\ i = 1\ldots 2n; \qquad \Delta\mathbb{X}_{k-1}^{(i)} = \left(\sqrt{nP_{k-1}^{+}}\right)_i^t,\ i = 1\ldots n; \qquad \Delta\mathbb{X}_{k-1}^{(n+i)} = \left(-\sqrt{nP_{k-1}^{+}}\right)_i^t\ i = 1\ldots n \tag{13}$$

in which $\left(\pm\sqrt{nP_{k-1}^{+}}\right)_i^t$ is the $i-th$ line of the state error covariance matrix. Those *sigma points* are propagated through the non-linear dynamics and updated as soon as new information is provided by the observation model in iterative steps, analogously to the linear Kalman filter. It is shown (Merwe and Wan, 2000) that the unscented transform renders the filter up to 3rd. order linearization accuracy, as compared to 1st. order of the EKF.

MATERIALS AND METHODS

A passenger car was equipped with two sets of sensors: Those on a smartphone Samsung Galaxy S7 Edge and, connected to an Arduino UNO with proper shield, a Hall-effect sensor KY-003, and a NEO6MV2 GPS; sensor's characteristics are summarised in Tab. 2. A permanent magnet attached to one of the wheels and the Hall sensor fixed to the body of the vehicle were used to measure the longitudinal speed; Altitude was calculated from barometer readings according to the barometer formula (Berberan-Santos, Bodunov, and Pogliani, 1997),

$$z^e = h_b + \frac{RT_b \log_e \frac{P}{P_b}}{-g_0 M}, \tag{14}$$

in which z^e is the vehicle's altitude, P is the barometer reading, R is the universal gas constant, h_b, T_b, P_b are respectively the altitude, standard temperature, and pressure at sea-level, g_0 is the acceleration of gravity, and M is the air molar mass. From barometer readings, altitude was computed taking into account, pressure and temperature from sea-level. An overall view of the setup is shown in Fig. 2.

Table 2: Sensor data: [1]UMI and [2] on Samsung phone; [3] stand-alone connected to Arduino.

Sensor	Type	Data	Max. sampl. rate	Range	Resolution	Unit
STM K6DS3TR[1]	3-axis accelerometer	acceleration	$500\,Hz$	± 8	2×10^{-4}	g
STM K6DS3TR[1]	3-axis gyro	angular speed	$500\,Hz$	± 1000	3.5×10^{-2}	$^o/s$
YAMAHA YAS537[2]	3-axis magnetometer	Earth mag. field	$100\,Hz$	± 1200	1.0×10^{-1}	μT
STM LPS25H[1]	barometer	atm. pressure	$10\,Hz$	± 1260	2.0×10^{-4}	hPa
HALL KY-003[3]	Hall-effect	near mag. field	–	–	–	–
NE06MV2[3]	GPS	position	$1\,Hz$	–	–	–

After installation and alignment of the UMI, the vehicle was turned on and maintained at rest during 30 s for calibration of sensors before travelling an approximate 370 m-long urban route, as shown in Fig. 4a, that took 90 s to run. UMI high-frequency sensor noise used as input to Kalman filters non-linear propagation model of Eq. 8 was low-pass filtered at

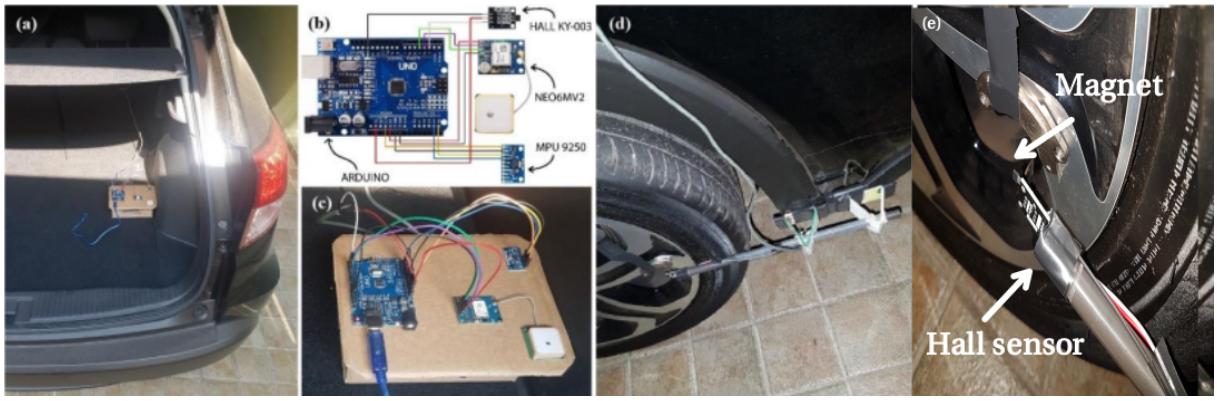

Figure 2: (a) Arduino UNO in the trunk of the vehicle; (b) Arduino connections diagram; (c) Arduino detail; (d) fixation of Hall sensor to the vehicle; (e) detail of Hall sensor and magnet attached to the wheel.

$1Hz$ cutoff frequency, as portrayed in Fig. 3. At the end of the run, the vehicle was once more kept at rest during 30 s to confirm the initial calibration. Phyphox 1.1.9 mobile app was used to acquire, record and transfer smartphone sensor data to a notebook computer. System and observation models were assumed uncorrelated; as a consequence, error covariance matrices $Q_{En,U}$ and $R_{En,U}$ respectively for the the EnKF and the UKF are diagonal, with the following variances:

$$Q_{En} = [10^{-4}\ 10^{-3}\ 10^{-4}\ \ 1\ \ 10^{2}\ 10^{2}\ 10^{-3}\ 10^{-3}\ \ 1\ 0.36\ \ 0.36\ 10^{-2}] \tag{15}$$

$$R_{En} = [0.25\ \ 0.01\ \ 0.01\ \ 1] \tag{16}$$

$$Q_{U} = [10^{-6}\ 10^{-5}\ 10^{-6}\ \ 4\ \ 1\ \ 25\ \ 10^{-4}\ 10^{-4}\ \ 25\ \ 4.10^{-3}\ \ 4.10^{-3}\ \ 10^{-4}] \tag{17}$$

$$R_{U} = [1\ \ 0.01\ \ 0.09\ \ 4] \tag{18}$$

Data processing and analysis were done in open-source software Scilab 6.1.0.

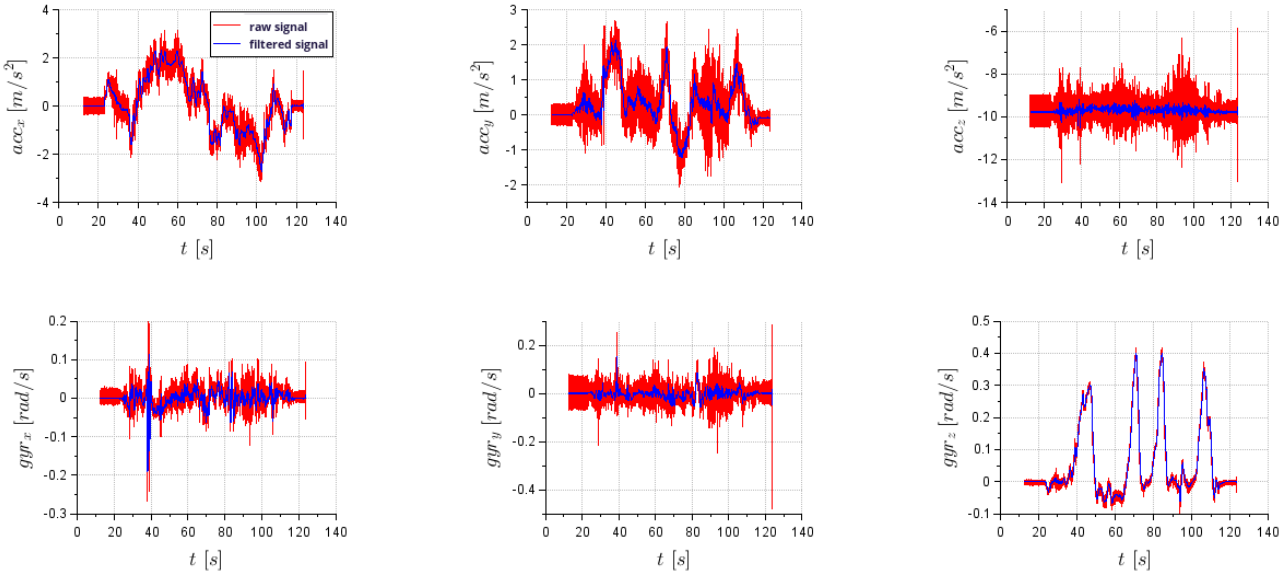

Figure 3: UMI accelerometer and gyro raw (red) and 1 Hz low-pass filtered (blue) data.

RESULTS AND DISCUSSION

Preliminary results of the experimental test with the vehicle in an urban route are depicted in Fig. 4b. It is noticeable that the blind propagation of the analytical model using sensor data without taking into account the stochastic nature of inherent measurement noise leads to an useless result, as the trajectory drifts away from the reference since the very beginning, even when the route is straight, and totally diverges soon after the first turn to the right.

On the other hand, it is possible to observe that the EnKF and the UKF fusing data from several sensors are capable of tracking the reference trajectory, despite a discrepancy that starts when the vehicle yaws the first time, reaching a

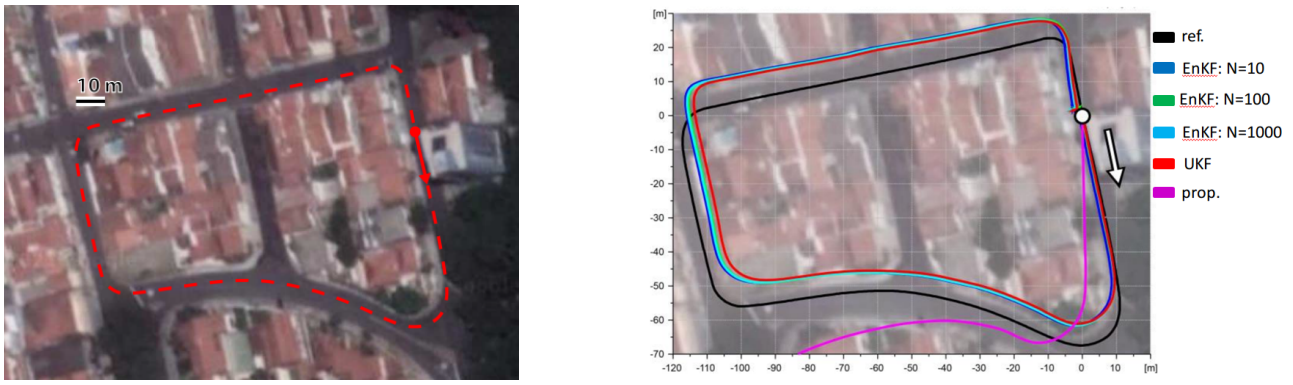

(a) (b)

Figure 4: Urban test route (a) map (adapted from Google Maps), with red dot and arrow indicating departure/arrival point and travel direction; (b) trajectories: reference, propagated and estimated by EnKF and UKF.

maximum of about 8 m. After that, the estimated and the reference tracks remain almost parallel, until the vehicle returns to the departure point, where a 2 m error is predicted by both filters. One should also point out that the EnKF and the UKF performances are similar, with a slight advantage for the EnKF. This statement can be corroborated by observing the traces in Fig. 4b and by comparing the Euclidean norms of the state error covariance matrices at the end of the test, as shown in Fig. 5: $\simeq 6$ for the EnKF and $\simeq 150$ to the UKF.

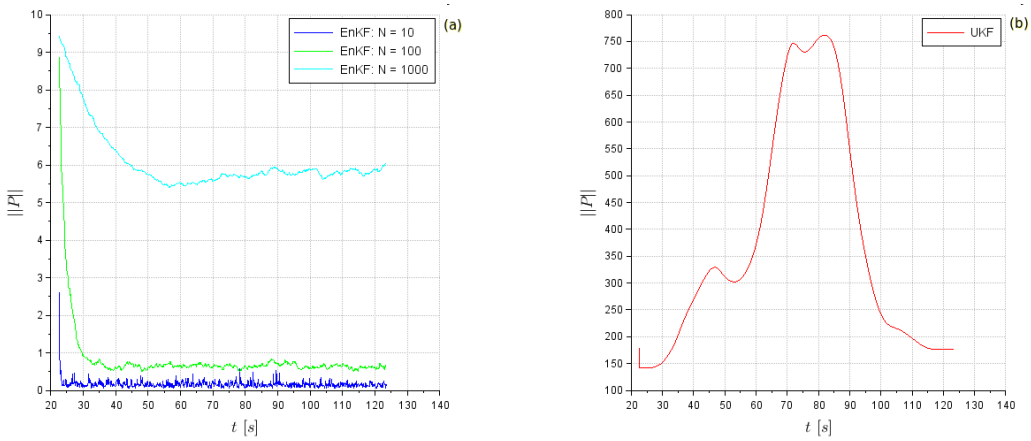

Figure 5: Estimation error covariance matrix norm (a) EnkF; (b) UKF

Still with respect to the EnKF, one might argue that the plot on Fig. 5(a) contradicts the previous assertion, since P-matrix Euclidean norm increases as the number of *ensembles* increases. This apparent paradox can be explained: In a stochastic sense, a smaller *ensemble* presents less dispersion than a bigger one, thus theoretically providing more accurate estimates. However, a small estimation error covariance may also occur when the filter converges well to a *wrong* state, hence characterising divergence. This way, although the filter apparently performs poorly on a larger ensemble, this fact helps the filter to remain open to new information from the array of sensors which, in turn, will be used to continuously improve the upcoming estimates.

The issue of convergence in Kalman filtering can be properly addressed by analysing the statistics of the observation residuals, defined as the difference between the measurements from sensors and the respective values obtained by the observation model processing the state estimated by the filter, *i. e.*,

$$\mathbb{r}_k = \mathbb{y}_k - H\hat{\mathbb{x}}_k \tag{19}$$

Convergence is achieved once the statistics of the observation residuals are the same as those admitted for the uncertainties of the system and observation models, in our case, zero-mean Gaussian, as it is confirmed by the respective histograms of both filters in Fig. 6.

The literature (Evensen, 2003) asserts that the estimates provided by the EnKF improve as the size of the *ensemble* increases. In our experiment, this behaviour is not significant, as depicted in Fig. 7, unless in relation to state variables

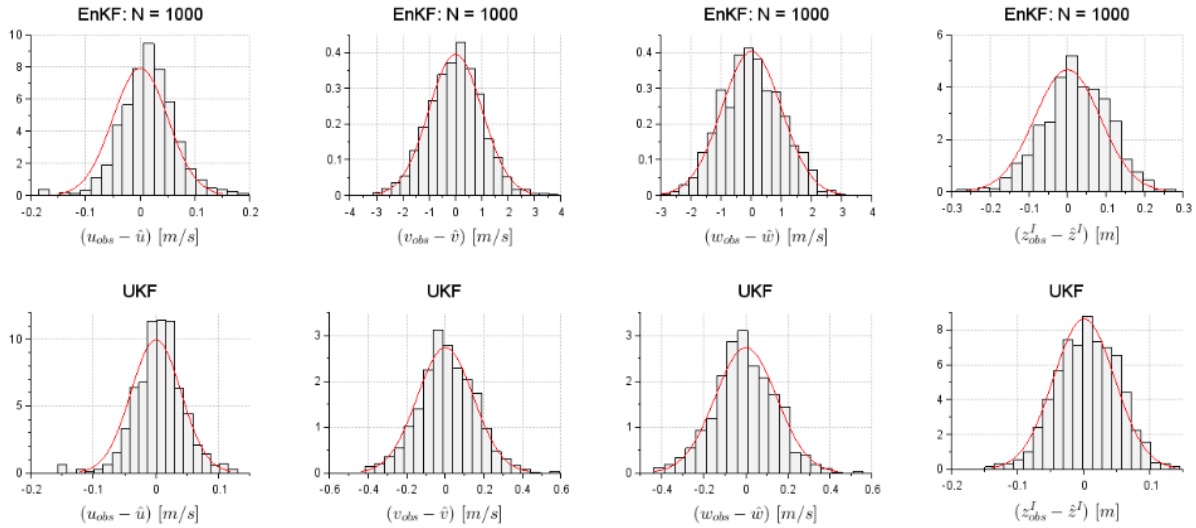

Figure 6: Probability distribution (grey) and zero-mean Gaussian reference curve (red) for the state variables.

roll (ϕ) and pitch (θ) angles, and lateral (v) and vertical (w) velocities. During the test, roll and pitch angles experienced minor random perturbations around zero, consistent with a random walk pattern; as a result, the larger the *ensemble*, the estimates come closer to a random walk with small dispersion (variance). The same rationale can explain the outcomes for lateral and vertical velocities, as one recalls that, by hypothesis, they were considered random walks. Possible reasons for the results obtained to the remaining variables u, x^e, y^e, z^e,, and ψ might include the reduced size of the *ensembles*, which has to be tuned for each application, the number of sensors fused, and the short duration of the test.

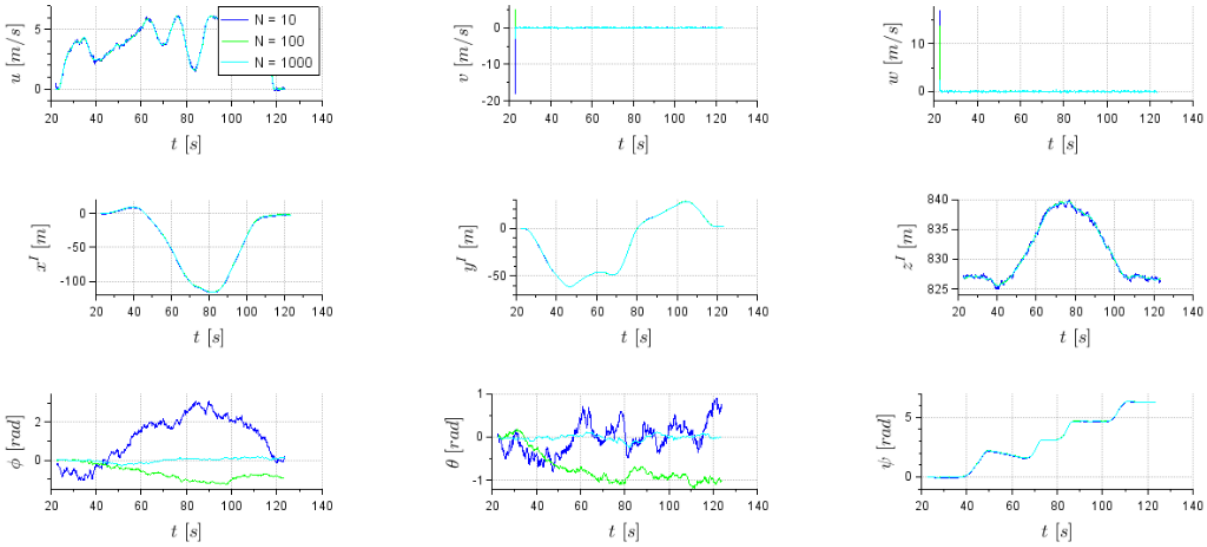

Figure 7: EnKF estimates as a function of the *ensemble* size.

CONCLUSION

Results of this work suggest that the Ensemble Kalman filter might be used as an alternative for the state estimation on dead reckoning using low-cost encapsulated inertial sensors (IMUs) in everyday applications as an alternative for the specialised gimballed devices. One could, however, argue that the filters converged to a state that is not as accurate as it was expected; in reply, we state that this research is ongoing in our group. One of the ideas we are exploring, in the Master's Thesis of the first author is the fusion of sensors from several IMUs (instead of just one, as presented in this paper) and adaptive filtering, in order to obtain optimised estimates. Another important aspect we are investigating is real-time processing of data in the EnkF, since there is a trade-off between estimates accuracy and *ensemble* size. A potential manner to address this issue is sequential processing of measurements, which is also under investigation by our group.

REFERENCES

Al-Shabi, M., and Bonny, T., 2022, "FPGA-based unscented Kalman filter for target tracking," Proc. SPIE 12122, Signal Processing, Sensor/Information Fusion, and Target Recognition XXXI.

Berberan-Santos, M.N., Bodunov, E.N. and Pogliani, L., 1997, "On the barometric formula," American Journal of Physics, 65(5), pp.404-412.

Evensen, G., 2003, "The Ensemble Kalman Filter: Theoretical Formulation and Practical Implementation," Ocean Dynamics (53): pp.343 - 367.

Julier, S.J. and Uhlmann, J.K., 1997, July, "New extension of the Kalman filter to nonlinear systems," *In*: Signal processing, sensor fusion, and target recognition VI (Vol. 3068, pp. 182-193). Spie.

Kochem, M., Wagner, N., Hamann, C.-D., Isermann, R., 2002, "Data fusion for precise dead-reckoning of passenger cars", IFAC Proceedings Volumes, Vol. 35, Issue 1, pp. 397-402.

Marco, V.R., Kalkkuhl, J., Raisch, J., Scholte, W.J., Nijmeijer, H. and Seel, T., 2020, "Multi-modal sensor fusion for highly accurate vehicle motion state estimation," Control Engineering Practice, 100, p.104409.

Maybeck, P.S., 1979, "Stochastic models, estimation, and control," Vol. 1, Academic Press, NY, USA, 445 p.

Oxley, A., 2017, "Positioning and navigation systems," *In*: Oxley, A. Uncertainties in GPS positioning: a mathematical discourse, Bahrain, Academic Print, Chap. 1, p. 1-18.

Park, S. and Hong, S.K., 2011, "Angular Rate Estimation Using a Distributed Set of Accelerometers," Sensors, vol. 11(11), pp. 10444-10457.

Sabattini, A. M., 2009, Dead-Reckoning Method for Personal Navigation Systems Using Kalman Filtering Techniques to Augment Inertial/Magnetic Sensing. Pisa: IntechOpen.

Shit, Rathin C.,2020, "Precise localization for achieving next-generation autonomous navigation: State-of-the-art, taxonomy and future prospects," Computer Communications, Vol. 160, pp. 351-374.

Scholte, W. J., Marco, V. R., and Nijmeijer, H., 2019, "Experimental validation of vehicle velocity, attitude and IMU bias estimation", IFAC-PapersOnLine, 52(8), 118-123.

Vargas-Meléndez, L., Boada, B.L., Boada, M.J.L, Gauchía, A. and Diaz, V., 2016, "A Sensor Fusion Method Based on an Integrated Neural Network and Kalman Filter for Vehicle Roll Angle Estimation," Sensors, 16(9) 1400, pp. 1-18.

Wan, E.A.; Merwe, R., 2000, "The unscented Kalman filter for nonlinear estimation," *In*: IEEE 2000 Adaptive Systems for Signal Processing, Communications, and Control Symposium, Proceedings [...]. IEEE, pp. 153-158.

RESPONSIBILITY NOTICE

The author(s) is (are) the only responsible for the printed material included in this paper.